Solar Light Induced Photon-Assisted Synthesis of TiO2 Supported Highly Dispersed Ru Nanoparticle Catalysts

Joanna Wojciechowska, Elisa Gitzhofer, Jacek Grams, Agnieszka Ruppert, Nicolas Keller

materials

MDPI

Article

Solar light induced photon-assisted synthesis of TiO_2 supported highly dispersed Ru nanoparticle catalysts

Joanna Wojciechowska[1,2], Elisa Gitzhofer[2], Jacek Grams[1], Agnieszka M. Ruppert[1], and Nicolas Keller[2,*]

[1] Institute of General and Ecological Chemistry, Faculty of Chemistry, Lodz University of Technology, ul. Żeromskiego 116, 90-924, Łódź, Poland ; agnieszka.ruppert@p.lodz.pl
[2] Institut de Chimie et Procédés pour l'Energie, l'Environnement et la Santé, CNRS/University of Strasbourg, 25 rue Becquerel, 67087 Strasbourg, France ; nkeller@unistra.fr
* Correspondence: nkeller@unistra.fr; Tel.: +33-3-6885-2811

Received: date; Accepted: date; Published: date

Abstract: Ru/TiO_2 are promising heterogeneous catalysts in different key-reactions taking place in the catalytic conversion of biomass towards fuel additives, biofuels or biochemicals. TiO_2 supported highly dispersed nanometric-size metallic Ru catalysts were prepared at room temperature *via* a solar light induced photon-assisted one-step synthesis in liquid phase, far smaller Ru nanoparticles with sharper size distribution being synthesized when compared to the catalysts prepared by impregnation with thermal reduction in hydrogen. The underlying strategy is based on the redox photoactivity of the TiO_2 semi-conductor support under solar light for allowing the reduction of metal ions pre-adsorbed at the host surface by photogenerated electrons from the conduction band of the semi-conductor in order to get a fine control in terms of size distribution and dispersion, with no need of chemical reductant, final thermal treatment or external hydrogen. Whether acetylacetonate or chloride was used as precursor, 0.6 nm sub-nanometric metallic Ru particles were synthesized on TiO_2 with a sharp size distribution at a low loading of 0.5 wt.%. Using the chloride precursor was necessary for preparing Ru/TiO_2 catalysts with a 0.8 nm sub-nanometric mean particle size at 5 wt.% loading, achieved in basic conditions for benefitting from the enhanced adsorption between the positively-charged chloro-complexes and the negatively-charged TiO_2 surface. Remarkably, within the 0.5-5 wt.% range, the Ru content had only a slight influence on the sub-nanometric particle size distribution, thanks to the implementation of suitable photo-assisted synthesis conditions. We demonstrated further that a fine control of the metal Ru nanoparticle size on the TiO_2 support was possible *via* a controlled nanocluster growth under irradiation, while the nanoparticles revealed a good resistance to thermal sintering.

Keywords: Ru/TiO_2 catalyst; catalyst preparation; sub-nanometric particle size distribution; highly dispersed Ru nanoparticle ; reaction mechanism; photodeposition; photon-assisted synthesis

1. Introduction

The crucial role played by heterogeneous catalysis in industrial chemical processes usually requires the engineering of tailored supported metal nanoparticles as catalysts, since the catalytic activity and the reaction rates can be strongly influenced by both the shape and the size of supported metallic nanoparticles [1-3]. A fine control over both the size and the size distribution of supported metal nanoparticles is necessary for increasing the metal dispersion for a given metal loading and improving the performances of catalytic reactions, as well as for investigating the

mechanisms taking place in size–dependent catalytic reactions thanks to the establishment of more detailed structure-properties relationship studies [4-6].

The solar light photon-assisted synthesis method is considered as a sustainable and elegant preparation method for synthesising well-defined and small-size supported metal nanoparticles, and for providing a control over their size, distribution and oxidation state [7]. Provided that the support carrier is a semi-conductor material, the underlying strategy relies on the use of the redox photo-activity of the semi-conductor support for promoting under appropriate light electrons from the valence to the conduction band of the semi-conductor, subsequently available for reducing metal ions adsorbed at the support surface. The low-temperature and one-step photon-assisted synthesis method differs from the most widely used preparation methods, for which a final post-deposition reduction/activation/ step is required to form the supported metallic particles after the metal precursor has been introduced onto the support carrier, and usually consisting either in a thermal treatment with the use of external hydrogen, or in a chemical reduction in solution with external reducing agent [8].

Although the influence of the synthesis parameters on the deposition rate and on the metallic nanoparticle shape and was investigated in some early studies [9], the photodeposition synthesis method has been mainly used for preparing catalytic and photocatalytic materials consisting in monometallic and more scarcely bimetallic particles dispersed on a medium or high surface area support. TiO_2 was the main semi-conductor support used, although other materials such as $BiVO_4$ or GaN:ZnO were also investigated, while Au [10,11], Pd [12], Ag [13,14], Pt [9,15], Rh [16], Cu [17,18], and Pt-Ag [19] were the most studied metals, using usually acetylacetonates, chlorides, nitrates, and chloric acids as metallic precursors.

The aim of this paper is to report on the use of a photodeposition method as alternative method to classical wet impregnation followed by final reduction in temperature under hydrogen for preparing Ru/TiO_2 catalysts. Indeed, Ru/TiO_2 are promising heterogeneous catalysts in different key-reactions taking place in the catalytic conversion of biomass towards biochemicals, including *e.g.* biofuels or fuel additives. Catalysts supported on TiO_2 were proved to be remarkably stable for biomass conversion reactions, while ruthenium is a metal of choice notably for hydrogenating biomass-derived molecules [20]. Till now, the synthesis of Ru nanoparticles at the surface of a support *via* a photodeposition method remained scarce, and was achieved using $(NH_4)_3RuCl_6$ or $RuCl_3$ as ruthenium salts, and TiO_2, CdS, CeO_2 and $CuInS_2$ quantum dots as host semiconductors under UV-vis or visible light irradiation [21-24].

Here we show that a one-step photon-assisted synthesis method can be implemented under simulated solar light for preparing Ru/TiO_2 catalysts with a Ru content ranging from 0.5 to 5 wt.%, with a sharp, nanometer-size and finely tunable Ru particle size distribution.

2. Materials and Methods

2.1 Ru/TiO_2 material preparation

Aeroxide© P25 TiO_2 (Evonik) has been used as TiO_2 support for preparing Ru/TiO_2 catalysts under simulated solar light irradiation. Ruthenium (III) acetylacetonate $(Ru(acac)_3$, 97%, Sigma-Aldrich) and ruthenium (III) chloride hydrate ($RuCl_3 \bullet xH_2O$, min 40% Ru content, Sigma-Aldrich) were used as ruthenium metallic precursors. Dissolution of the $Ru(acac)_3$ precursor was achieved in distilled water under stirring at 50°C for 2 days, whereas the $RuCl_3$ precursor was dissolved under stirring in 10 ml of methanol for 12 h, prior to the addition of 90 ml of distilled water to give a methanol:water ratio of 1:9 v/v. In each experiment, the TiO_2 support was dispersed under stirring in 100 mL of ruthenium solution in a beaker-type glass reactor at a 1 g/L concentration, with a precursor concentration depending on the targeted Ru content to be achieved in the final Ru/TiO_2 material. Prior to irradiation, the suspension was stirred in the dark for 2 h to ensure the establishment of the adsorption-desorption equilibrium. In the case of $Ru(acac)_3$, the pH value of the suspension was adjusted with NaOH to pH=10, whereas for higher Ru loading (5%)

using $RuCl_3$ the pH was adjusted with NaOH to pH=8. The TiO_2 suspension was further exposed under stirring to a 500 W/m² solar light irradiation within an ATLAS Suntest XLS+ reaction chamber equipped with a Xenon arc lamp NXE 2201.

At each time interval, 1 mL of solution was sampled and filtrated through a 0.20 μm porosity filter (Aireka Cells) to remove the titania powder if any. The deposition was followed by UV-vis spectrophotometry using a Cary 100 Scan Varian spectrophotometer monitoring the disappearance of the main absorption peak at λ=272 nm and λ=324 nm for $Ru(acac)_3$ and $RuCl_3$ precursors, respectively. After completion of the process, the catalysts were recovered by filtration and dried at 100°C for 1 h.

2.2. Characterisations

The Ru content in the catalysts was determined by chemical analysis after a microwave-assisted acidic dissolution in aqua regia at 185°C under autogenic pressure. Inductively coupled plasma optical emission spectroscopy (ICP-OES) was carried out on an Optima 7000 DV spectrometer (Perkin Elmer) at the Analysis Plateform of IPHC-Strasbourg, France.

The Ru nanoparticle size distribution of Ru/TiO_2 samples was determined by transmission electron microscopy (TEM) performed using a JEOL 2100F with a point resolution of 0.2 nm. The samples were sonically dispersed in an ethanol solution before a drop of the solution was deposited onto a copper grid covered by a holey carbon membrane for observation. The size distributions were calculated for each sample by averaging 300 particles from the TEM images using ImageJ software.

X-Ray Photoelectron Spectroscopy (XPS) characterization was performed on a ThermoVGMultilabESCA3000 spectrometer equipped with an Al K_α anode ($h\lambda$ = 1486.6 eV). The energy shift due to electrostatic charging was subtracted using the adventious sp^2 carbon C 1s band at 284.6 eV. The spectra were decomposed assuming several contributions, each of them having a Doniach–Sunjic shape [25] and a' S-shaped' Shirley type background [26]. Surface atomic ratios were derived using the appropriate experimental sensitivity factors [27].

Thermogravimetric analysis (TGA) was carried out with a 20% (v/v) O_2/N_2 mixture at a flow rate of 40 mL/min at a heating rate of 10°C/min from 25°C to 600°C using a Q 5000 TA Instrument thermoanalyzer.

3. Results and discussion

3.1. Influence of the Ru metallic precursor and of the targeted Ru content

$Ru(acac)_3$ and hydrated $RuCl_3$ are the most used Ru precursors allowing the preparation of supported Ru catalysts on a wide variety of supports *via* wet or wetness impregnation with final thermal reduction under hydrogen, so that they both have been used as metallic precursors for preparing a series of ruthenium catalysts with a targeted nominal Ru content from 0.5 wt.% to 5 wt.%.

Figure 1 shows the disappearance with time under illumination of both Ru metallic precursors using TiO_2 P25 as semi-conductor host support. First, photolysis of the ruthenium precursors could be neglected under solar light in our experimental conditions, since no disappearance of the main absorption peaks assigned to both precursors was observed whatever the precursor used (not shown). The evolution with time of the relative concentration evidenced that both the Ru concentration and the Ru precursor nature are strongly influencing the kinetics of the photocatalytic degradation of the $Ru(acac)_3$ and of the $RuCl_3$ species at the surface of the irradiated TiO_2 support. Whatever the Ru content, a slower degradation was observed with the acetylacetonate compared to the chloride precursor. Indeed, at a content of 0.5 wt.%, a reaction time greater than 200 min was needed for achieving the complete disappearance of the Ru precursor using acetylacetonate, while only 100 min was necessary using the chloride precursor. Table 1 shows the real metal content of selected Ru/TiO_2 catalysts after the photon-assisted synthesis, with a

close agreement being observed between the measured Ru content and the theoretical one derived from the UV-vis absorbance spectra evolution.

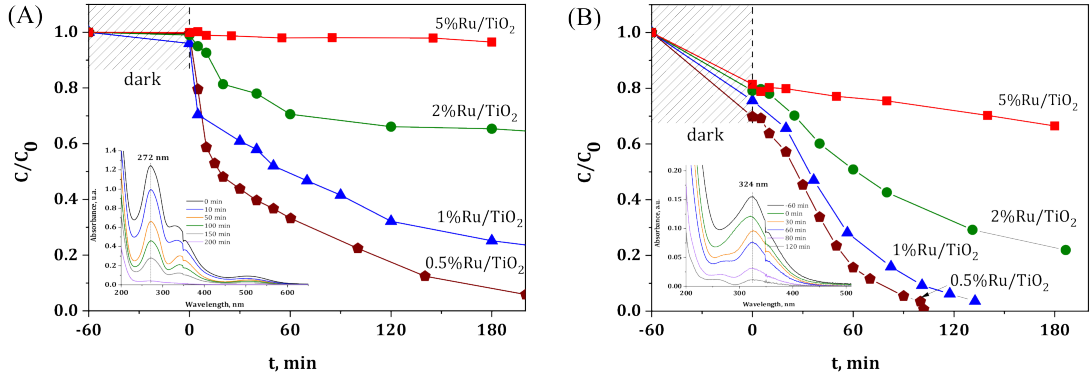

Figure 1. Disappearance of the Ru precursor in the presence of TiO_2-P25 as a function of the illumination time for **(A)** $Ru(acac)_3$ and **(B)** $RuCl_3$ precursors, with a Ru concentration ranging from 0.5 to 5 wt.%. Inset: UV-vis absorbance spectra evolution as a function of time during the photon-assisted synthesis for 0.5 wt.% of Ru.

For both Ru precursors, increasing the Ru concentration led to increase the necessary reaction time, the effect being more pronounced using acetylacetonate. Indeed, targeting a Ru content of 2 wt.% led only to a photodeposition yield of 35%, where no photodeposition was observed for a Ru concentration of 5 wt.%. Even in the case of the chloride precursor for which faster kinetics have been observed, the preparation of highly loaded Ru/TiO_2 catalyst with loadings higher than 2 wt.% could not be achieved within a reasonable time under irradiation.

Table 1. Ru content in Ru/TiO_2 materials determined by ICP-OES

Ruthenium precursor, pH	Targeted Ru content, wt.%	Ru content, wt.%[a]
acetylacetonate	0.5	0.45
chloride, 4.4	0.5	0.46
chloride, 6.4	1	0.92
chloride, 8.0	5	4.9
chloride, 6.4	5	4.8

[a] a maximum of about 10% relative difference was observed between the measured Ru content and the theoretical one derived from the UV-vis absorbance profile, demonstrating that the direct monitoring of the Ru precursor disappearance by UV-Vis spectrophotometry was a fast and suitable method for obtaining the Ru content in the catalysts.

3.2. Characterization of the Ru(0.5 wt.%)/TiO_2 catalysts

TEM images with the derived histograms of the Ru nanoparticle size distribution for Ru/TiO_2 catalysts prepared with both $Ru(acac)_3$ and $RuCl_3$ metallic precursors with a Ru concentration of 0.5 wt.% are shown in Figure 2.

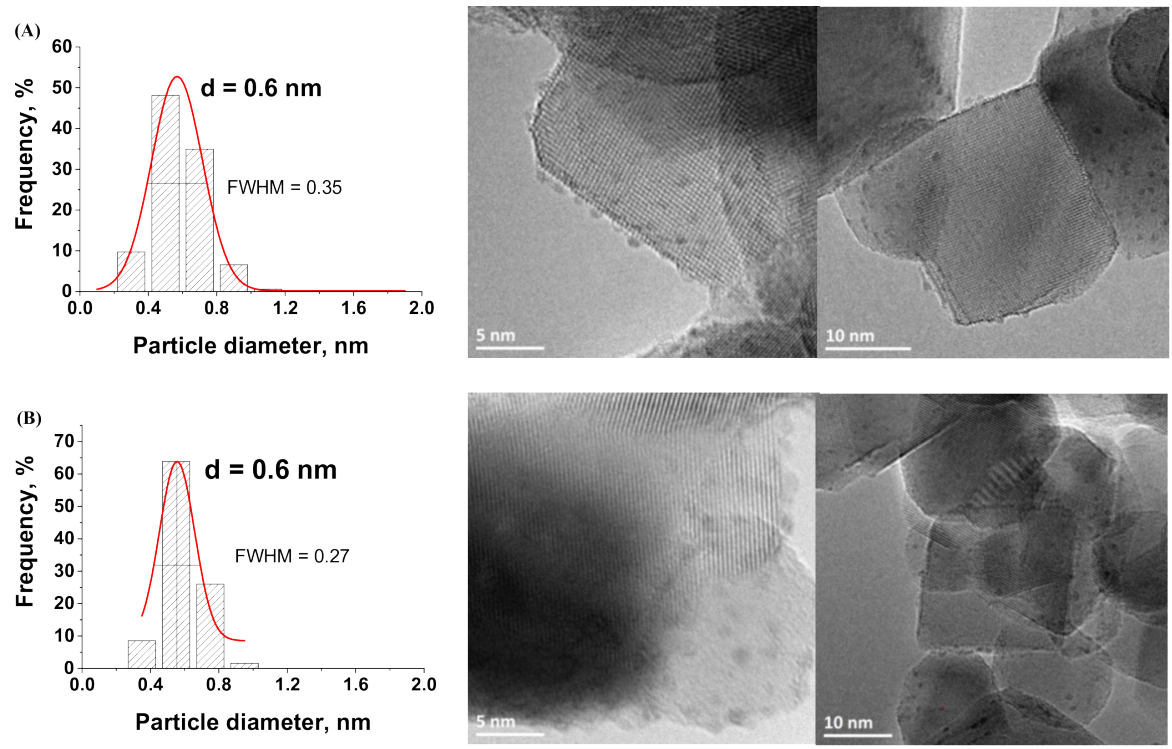

Figure 2. TEM images with the derived histograms of the Ru nanoparticle size distribution for the Ru(0.5 wt.%)/TiO_2-P25 catalysts prepared from **(A)** acac and **(B)** chloride.

Whether the chloride or the acetylacetonate form of the Ru metallic precursor was used, the nanoparticles synthesized on the TiO_2 support were dispersed homogeneously and no Ru nanoparticle aggregates were observed. Although both precursors strongly differ in terms of chemical nature, small Ru nanoparticles were synthesized on the TiO_2 support with a similar sharp sub-nanometric particle size distribution centered on 0.6 nm in both cases. A slightly sharper nanoparticle size distribution was obtained using the chloride precursor compared to that obtained with the acetylacetonate counterpart, with a Full Width at Half Maximum (FWHM) of 0.27 *vs.* 0.35.

XPS surface characterization and high resolution TEM analysis confirmed the metallic nature of the Ru nanoparticles synthesized on the TiO_2 support (Figure 3). Whatever the Ru precursor used, contributions attributed to both metallic Ru^0 (484.1 eV) and Ru^{4+} (488.7 eV) species were observed in the Ru $3p_{1/2}$ orbital XPS spectra of Ru(0.5 wt.%)/TiO_2 [29]. Within a more complex multi-contribution envelope resulting from the binding energy overlap between Ru 3d and C 1s XPS spectra, the Ru 3d spectra confirmed the presence of both Ru^0 and Ru^{4+} species, with the presence of two Ru $3d_{5/2}$ - Ru $3d_{3/2}$ orbital doublet contributions at 280.2 eV and 281.9 eV with a 4.1 eV spin orbit splitting, in addition to the contributions due to the adventious carbon.[28]

It was noteworthy that both the ratio of atomic concentrations between Ru^0 and Ru^{4+} (estimated at 70/30 ± 7 by combining both Ru 3d and Ru 3p spectra results) and the Ru/Ti surface atomic ratio calculated at *ca.* 0.02 were not influenced by the kind of precursor used. This confirmed that both Ru nanoparticle size distribution and the Ru oxidation state at the TiO_2 surface were not affected by the choice of the metallic precursor.

In addition, an interplane distance of 2.1 Å corresponding to the (101) atomic planes of metallic Ru was measured on TEM images.[29] The mean Ru nanoparticle size derived from TEM images being of 0.6 nm, the Ru nanoparticles supported on TiO_2 could be considered in a first approximation as being composed in average of only about 3-4 atomic layers. Considering the Ru^0/Ru^{4+} surface atomic ratio, we propose that the Ru^{4+} species related to the presence of one monolayer resulting from a natural surface oxidation of the metallic Ru nanoparticle, as observed for many supported noble metals. [30]. No presence of any residual chlorine was observed by XPS at the surface of TiO_2 when the chloride precursor was used (Cl 2p XPS spectra not shown).

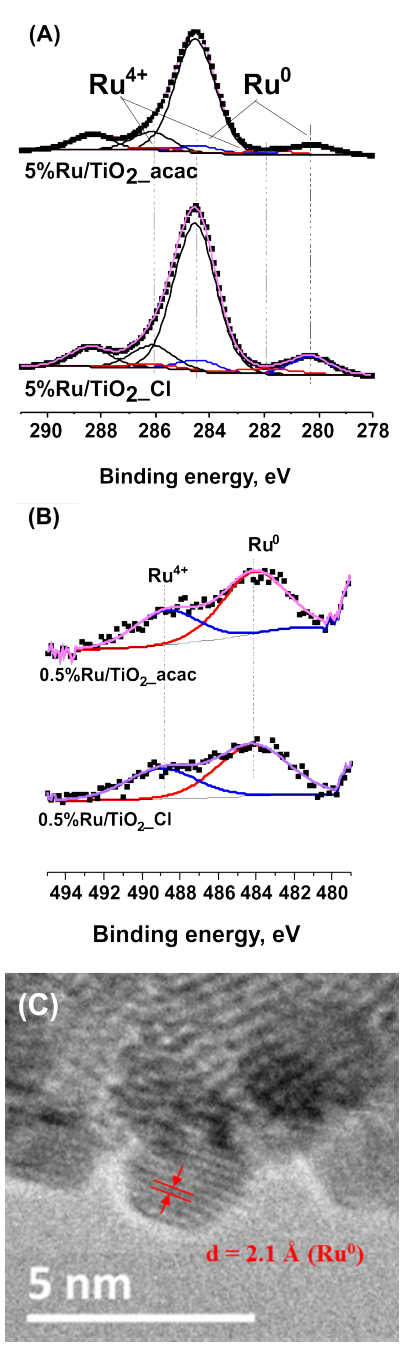

Figure 3. (A) Ru 3p and **(B)** Ru 3d + C 1s XPS profile of the Ru(0.5 wt.%)/TiO_2-P25 catalyst [31]. The carbon C 1s spectra was fitted with major contribution at 284.6 eV corresponding to graphitic sp^2 carbon and contributions attributed to oxygenated surface groups ; **(C)** TEM image of Ru(0.5 wt.%)/TiO_2-P25 with the measured interplane distance of (101) planes of metallic Ru.

The different behavior in terms of degradation kinetics observed on TiO_2 depending on the nature of the Ru metallic precursor used led to propose that the photon-assisted synthesis of Ru nanoparticles on TiO_2 occurred *via* two different mechanisms, as it was supported by a previous mechanistic study [31].

In the case of the $RuCl_3$ precursor, the photogenerated holes would not be involved in the mechanism proposed, that would only use the photogenerated electrons for obtaining the reduced metallic form of Cu, as the $RuCl_3$ precursor is present in aqueous solution as a mixture of Ru chloro-complexes.[32,33,34] By contrast, the mechanism proposed in the case of the acetylacetonate precursor involves both holes and electrons charge carriers in oxidation and reduction steps, respectively, and is derived from the study of Naya et al. on the photon-assisted synthesis of Cu

nanoparticles supported on $BiVO_4$ photocatalysts from Cu acetylacetonate [34] and schematized in Eqs. (1)-(4).

The Ru acetylacetonate adsorbed at the TiO_2 surface can be oxidized by OH° hydroxyl radicals formed *via* the oxidation of adsorbed water or of surface –OH groups by the photogenerated holes from the valence band, or directly by the holes. Although solar light was used as incident light, only its UV-A fraction activated the Aeroxide© P25 TiO_2 support and consequently generated the electron/hole pairs, due to the 3.2 eV band gap energy of the main anatase phase of the material.

$$TiO_2 + Ru(acac)_3 \leftrightarrow Ru(acac)_{3ad} \cdots TiO_2 \quad (1)$$

$$TiO_2 + hv \rightarrow e^- + h^+ \quad \text{(UV-A fraction of solar light)} \quad (2)$$

$$Ru(acac)_{3ad} + 3h^+ \rightarrow Ru^{3+} + (acac)_{ox} + H^+ \quad (3)$$

$$Ru^{3+} + 3e^- \rightarrow Ru^0 \quad (4)$$

The ligand oxidation would generate adsorbed Ru^{3+} ions that can further be reduced into metallic Ru by the photogenerated electrons from the conduction band. As far as Cu was concerned, the direct reduction of $Cu(acac)_2$ into metallic Cu was reported to be strongly unfavored compared to that of Cu^{2+}.[35] Total Organic Carbon measurements showed that the acetylacetonate ligand was mineralized into CO_2 with a 35% yield at the end of the photo-assisted synthesis process in the case of a 0.5 wt.% Ru content. It was proposed that the acetylacetonate ligand oxidation might follow a usual oxidation pathway for carboned molecules, with consecutive oxidation steps leading to form first partially-oxidized carboned molecules and further short-chain acids, and allowing progressively the complete substrate mineralization into CO_2 to be achieved. The presence of small amounts of carbon-containing reaction intermediate species at the surface of the Ru/TiO_2 resulting from the ligand oxidation was confirmed by TGA analysis, with a higher weight loss attributed to the desorption and the combustion of those species when using acetylacetonate compared to that observed on the material prepared with chloride (Figure 4).

However, considering the presence at the TiO_2 surface of oxidative species in addition to the photogenerated electrons, we could not fully rule out that the Ru^{4+} surface monolayer observed was formed during the synthesis *via* the *in situ* oxidation of Ru^0 by the photogenerated holes from the valence band or by hydroxyl radicals.

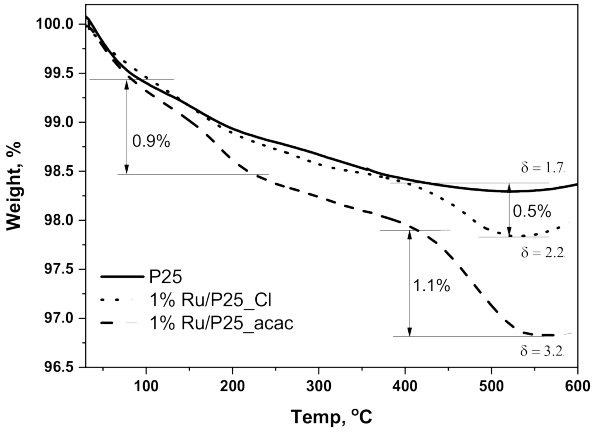

Figure 4. TGA profiles of TiO_2 P25 and 1%Ru/TiO_2 materials prepared from $Ru(acac)_3$ and hydrated $RuCl_3$ precursors. The weight loss observed on the reference TiO_2 sample, corresponded to the desorption of molecularly adsorbed water at low temperature and to the surface dehydroxylation (dehydration) at higher temperature. The additional weight loss recorded on the 1%Ru/TiO_2 materials prepared from $RuCl_3$, corresponded to the combustion of carbonaceous residues issued from the partial oxidation of methanol.

3.3. Influence of the precursor solution pH and preparation of the Ru(5 wt.%)/TiO_2 catalyst

Figure 5a shows the influence of the pH of the aqueous Ru precursor solution on the photodeposition kinetics of 0.5 wt.% Ru on TiO_2. It was worth noting that increasing the pH led to significantly enhance the adsorption of the Ru precursor species on the TiO_2 support in the dark, while reducing strongly the time necessary for a complete precursor disappearance, and consequently for preparing the Ru(0.5 wt.%)/TiO_2 material. This behavior with increasing the pH of the solution has been attributed to the amphoteric nature of the TiO_2 support, for which the surface is negatively-charged for pH higher that the zero-charge point (*ie.* ca. 6.25 for TiO_2-P25), and positively-charged for pH lower that the zero-charge point [36]. Thus, the TiO_2 surface is considered to be negatively-charged when the photodeposition was performed at pH=8, whereas the surface charge increased gradually with decreasing the solution pH, so that the reaction was implemented on a zero charge surface at pH 6.4, and on a positively-charged surface at pH=2.

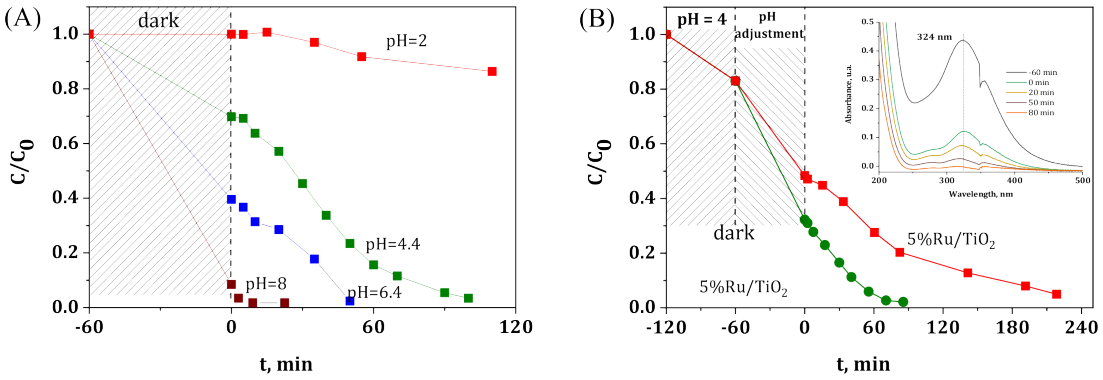

Figure 5. (A) Influence of the solution pH on the disappearance of the $RuCl_3$ precursor in the presence of TiO_2-P25 as a function of the illumination time for a Ru content of 0.5 wt.%. **(B)** Disappearance of the $RuCl_3$ precursor in the presence of TiO_2-P25 as a function of the illumination time at pH=6.4 and pH=8.0, with a Ru content of 5 wt.%. Inset: UV-vis absorbance spectra evolution as a function of time during the photon-assisted synthesis of Ru(5 wt.%)/TiO_2 at pH=8.

In water, $RuCl_3$ species are very complex systems and co-exists in the form of various aqueous chloro-complexes, for which the thermodynamic equilibrium depends on parameters like the pH, temperature and the concentration.[32] The determination of Ru forms in solution remains however very challenging, due to the multiple degrees of polymerization of the Ru chloro complexes as well as the co-existence of different oxidation states for Ru.[37] Considering the aqueous Ru chloro-complexes distribution diagrams with the chloride concentration evolution, we could propose to rule out the existence of negatively-charged Ru complexes like $RuCl_6^{3-}$, $RuCl_5(H_2O)^{2-}$ and $RuCl_4(H_2O)_2^{-}$ in the TiO_2 suspension, and we assumed that the Ru species are most probably present as a mixture of $RuCl_3(H_2O)_3$, and of positively-charged $RuCl_2(H_2O)_4^{+}$ and $RuCl(H_2O)_5^{2+}$ species. [33,34]

As a result, at low pH, the adsorption of Ru species on the positively-charged TiO_2 surface was unfavored due to electrostatic repulsion, while by contrast the increase in the solution pH above the isoelectrical point strongly enhanced the adsorption of Ru species on the positively-charged TiO_2 surface.

The strong influence of the pH on the adsorption behavior and consequently on the photodeposition kinetics opened the possibility of preparing Ru/TiO_2 catalysts with a high Ru metal loading of 5 wt.%, as shown in Figure 5b and in Table 1. At a higher Ru loading, a similar pattern was obtained, with a higher adsorption on the TiO_2 support at pH 8 compared to that observed at pH 6.4, so that a reaction time greater than 200 min was needed for achieving the complete precursor disappearance at pH 6.4, while only 90 min was necessary at pH 8.

3.4. Characterization of the Ru(5 wt.%)/TiO_2 catalyst

Figure 6 shows the TEM images and the derived histograms of the Ru nanoparticle size distribution for the Ru(5 wt.%)/TiO_2 catalyst prepared at pH=8.0 and pH=6.4. First, in both cases the supported nanoparticles were dispersed homogeneously and no Ru aggregates were observed. Small and sharp nanoparticle size distributions were obtained, centered on 0.8 nm (FWHM= 0.34 nm) and 1.0 nm (FWHM= 0.70 nm) at pH=8,0 and pH=6.4, respectively. The slightly smaller and sharper particle size distribution achieved at pH=8.0 was attributed to the higher adsorption of the aqueous Ru chloro-complexes with the negatively-charged TiO_2 surface at this pH, that led to maintain a higher and more narrow dispersion at the support surface. When performing the reaction at pH 8, it is remarkable that the increase in the Ru content by an order of magnitude did not result neither in a strong increase in the average particle size, nor in its broadening.

The metallic nature of the supported nanoparticles of the Ru(5 wt.%)/TiO_2 catalyst was confirmed by the high resolution TEM image (insert of Figure 6a) that evidenced an interplane distance of 2.1 Å corresponding to the (101) atomic planes of metallic Ru, as well as by XPS surface characterization (Figure 7). The Ru $3p_{1/2}$ and Ru $3d_{5/2}$ - Ru $3d_{3/2}$ orbital XPS spectra exhibited similar patterns than those recorded on the TiO_2 support with a low 0.5 wt.% of Ru. The Ru^0/Ru^{4+} atomic concentration ratio was estimated at 80/20 ± 7. The XPS patterns differed only in terms of intensity of both Ru^0 and Ru^{4+} doublets for the 3d orbitals in respect to the C1s main peak at 284.6 eV attributed to contamination carbon, and consequently in terms of Ru/Ti surface atomic ratio. The surface atomic ratio was calculated at 0.23 for 5 wt.% of Ru *vs.* 0.02 for 0.5 wt.% of Ru. The approximatively ten-fold higher ratio while increasing the Ru loading by an order of magnitude, characterized the maintain of a very high dispersion of small size Ru nanoparticles at the TiO_2 support surface confirmed the slight increase in mean particle size from 0.6 nm to 0.8 nm and the slight increase in FHWM from 0.27 nm to 0.34 nm.

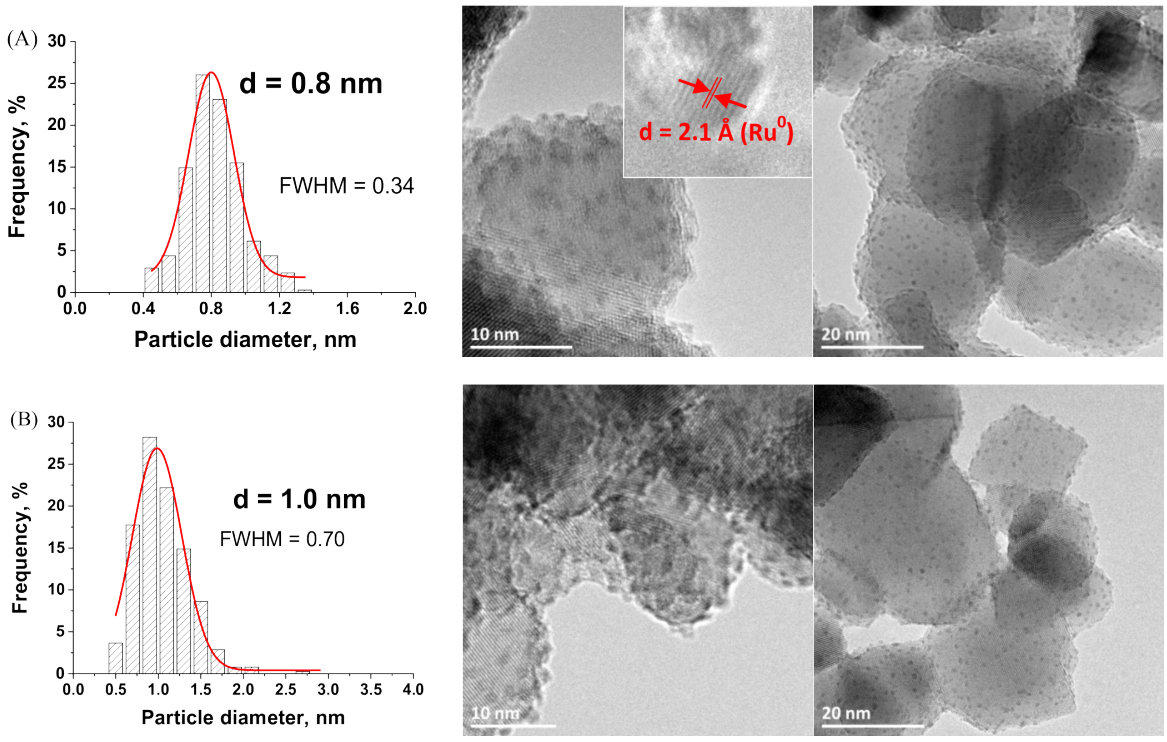

Figure 6. TEM image and the Ru nanoparticle size distribution for the Ru(5wt.%)/TiO_2-P25 catalysts prepared **(A)** at pH=8,0 with the measured interplane distance of (101) planes of metallic Ru ; and **(B)** pH=6.4.

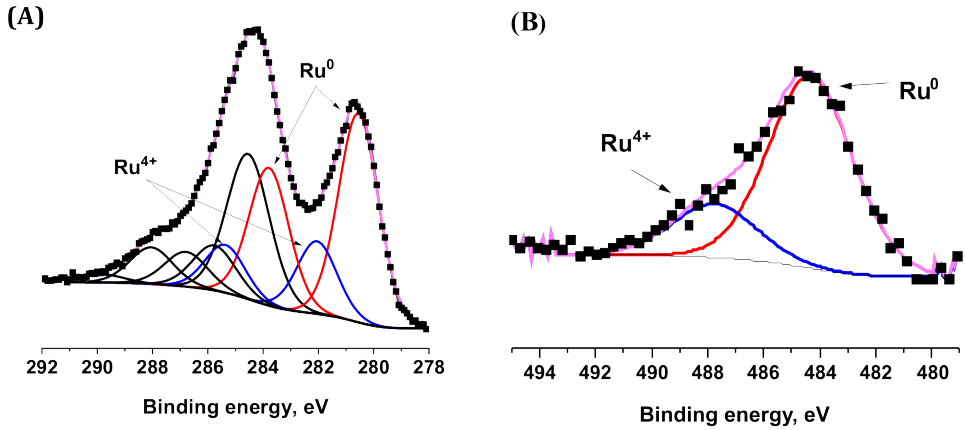

Figure 7. A) Ru 3d + C 1s ; **B)** Ru 3p XPS profile of the Ru(5 wt.%)/TiO_2-P25 catalyst. No presence of any residual chlorine was observed by XPS at the surface of TiO_2 when the chloride precursor was used (Cl 2p XPS spectra not shown).

This highlighted the interest of the synthesis method for preparing Ru/TiO_2 catalysts with well-calibrated Ru nanoparticles dispersed at the surface of the TiO_2 support. This contrasted with the Ru(5 wt.%)/TiO_2-P25 catalysts prepared *via* classical impregnation with final reduction under hydrogen at 200°C, that exhibited a broader nanoparticle size distribution (FHWM=1.86) centered on a larger average particle size, at 2.9 nm (Figure 8).

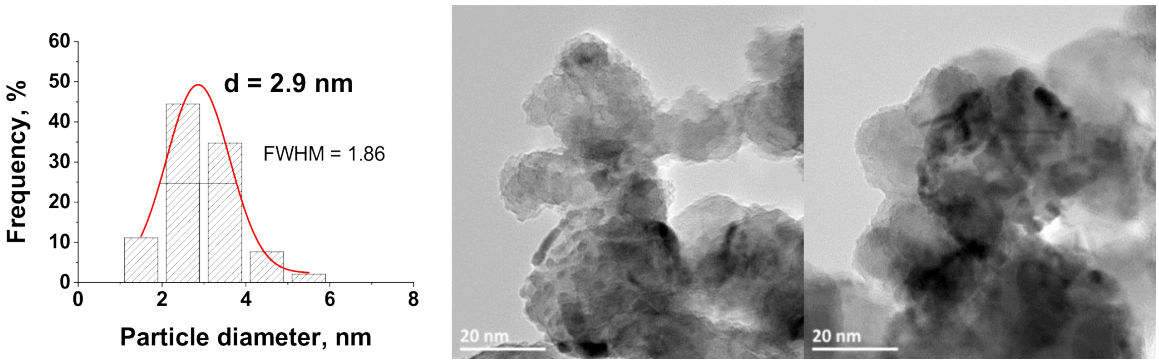

Figure 8. TEM image and the Ru nanoparticle size distribution for the Ru(5 wt.%)/TiO_2-P25 catalyst prepared *via* classical impregnation with final reduction in hydrogen at 200°C.

3.5. Fine control of the Ru particle size distribution

It has been further demonstrated that a fine monitoring of the metal Ru particle size on the TiO_2 support was possible *via* a controlled growth of the Ru nanoclusters under irradiation, achieved by extending the duration of the irradiation after the full conversion of the Ru precursor salt was achieved. Indeed, Figure 9 shows that the mean Ru particle size progressively and slightly increased from 0.6 nm to 0.9 nm and further to 1.1 nm, when 2 h and 6 h of supplementary irradiation time was provided to the system, respectively. Simultaneously, the FWHM values slightly increased from 0.25 nm to 0.52 nm and further to 0.62 nm, evidencing a slight broadening of the particle size distribution. Whatever the irradiation time, the nanoparticles remained homogeneously dispersed on the support with a small mean particle size and without the formation of large Ru nanoparticle aggregates. This highlighted the possibility to provide on-demand Ru/TiO_2 catalysts with a monomodal particle size distribution and a well-calibrated mean particle size for studying and optimizing the reactivity of heterogeneous catalysts in different size-dependent or structure-sensitive reactions [5,6].

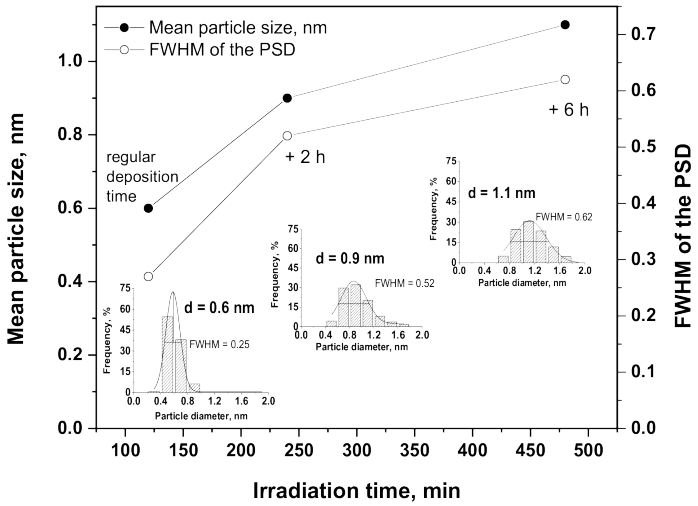

Figure 9. Evolution of the mean Ru particle size and of the distribution FWHM as a function of the irradiation time for the 1%Ru/TiO_2 catalyst prepared with the chloride precursor. Inset: Ru particle size distributions obtained for 2 h, 4 h and 8 h of irradiation, corresponding to the regular irradiation time, and 2 h and 6 h of extra-time irradiation in the absence of Ru precursor, respectively.

3.6 Influence of thermal reduction

The stability of the Ru(5 wt.%)/TiO_2 catalyst has been evaluated by submitting the as-prepared catalysts to further reduction under hydrogen at 200°C for 1 h. Those conditions are classical conditions for getting metallic Ru nanoparticles on supports such as *eg.* titania, activated carbon, alumina or zirconia by classical incipient wetness or wet impregnation with acetylacetonate or chloride precursors. [29,36,38]. In addition, many reactions involved in the catalytic conversion of biomass-derived molecules on Ru catalysts are also implemented at temperatures lower than 200°C [39], so that 200°C remains an appropriate temperature for evaluating the thermal stability of the catalysts. Figure 10 shows the TEM images with the derived histograms of the Ru nanoparticle size distribution for the treated Ru/TiO_2-P25 catalyst.

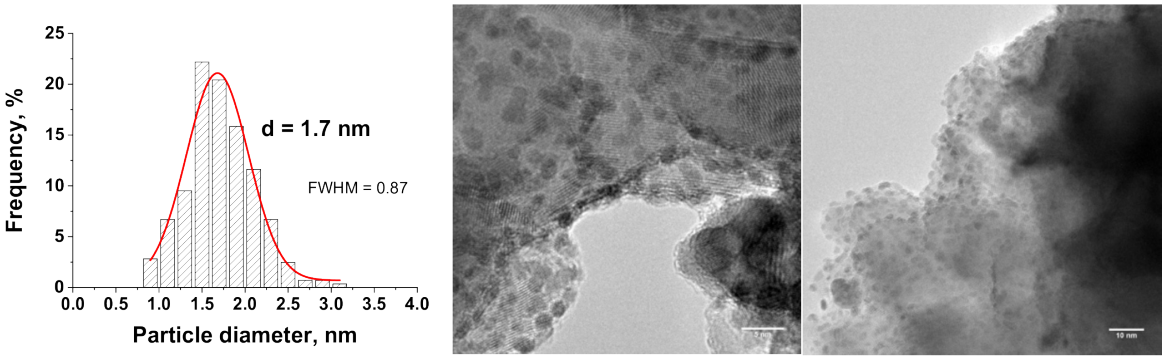

Figure 10. TEM images with the derived histograms of the Ru nanoparticle size distribution for the Ru(5 wt.%)/TiO_2-P25 catalyst obtained by the photon-assisted preparation method, after treatment at 200°C under hydrogen for 2 h.

It has been evidenced that the Ru(5 wt.%)/TiO_2 catalyst displayed a good resistance to nanoparticle sintering and growth. Indeed, the mean Ru particle size slightly increased from 0.8 nm to 1.7 nm, with a slight broadening of the distribution from 0.27 nm to 0.87 nm in terms of FWHM values. The nanoparticles remained homogeneously dispersed on the support with a small mean

particle size still far lower and a particle size distribution still far sharper to those obtained on the Ru(5 wt.%)/TiO_2 catalyst prepared *via* classical impregnation with reduction in H_2 at 200°C.

4. Conclusion

In this study, we proved the effectiveness of an elegant low-temperature one-step photon-assisted synthesis method taking advantage of the redox photoactivity of the TiO_2 semi-conductor support under solar light, for preparing highly dispersed TiO_2 supported metallic Ru catalysts that are promising heterogeneous catalysts in different key-reactions involved in the catalytic biomass conversion into fuel additives, biofuels or biochemicals. They exhibited an enhanced catalytic activity in the combined hydrogenation of levulinic acid into γ-valerolactone using formic acid as internal hydrogen source, as well as in the levulinic acid hydrogenation with external hydrogen, in comparison to that shown by the reference counterpart catalysts prepared by incipient wet impregnation [40]. This was possible thanks to the stabilization of well-dispersed, small and uniform metal crystallites.

Far smaller Ru nanoparticles with sharper size distribution were synthesized when compared to the catalysts prepared *via* wet or incipient wetness impregnation with final thermal reduction in hydrogen. While XPS and TEM analyses evidenced the highly dispersed and metallic state of the Ru nanoparticles, we have demonstrated that by implementing a suitable photo-assisted synthesis protocol, the size distribution of the supported sub-nanometric size Ru nanoparticles was only very slightly influenced by the Ru content within a large 0.5-5 wt.% range. Further, a fine monitoring of the metal Ru nanoparticle size on the TiO_2 support was possible *via* a controlled growth of the Ru nanoclusters under irradiation. Those catalysts exhibited a good resistance to thermally-activated nanoparticle sintering. This opens the possibility to prepare on-demand Ru/TiO_2 catalysts with a monomodal and well-calibrated particle size distribution for performing fundamental investigation on the reactivity of heterogeneous catalysts in different size-dependent or structure-sensitive reactions.

Author Contributions Statement: NK designed the research project. AR and NK supervised the study. JW and EG performed the experiments. JW and NK analyzed the data. JW conceived the figures. JW and NK wrote the manuscript. JW, JG, AR and NK finalized the manuscript.

Funding: This research received no external funding.

Acknowledgments: The French Embassy in Poland is acknowledged for supporting the PhD work of J.W. *via* a French Government Grant. D. Ihiawakrim (IPCMS, Strasbourg) is thanked for performing TEM analysis.

Conflicts of Interest: The authors declare no conflict of interest.

References

1. Nigam PS, Singh A. Production of liquid biofuels from renewable resources. Prog. Energy Combust. Sci. (2011) 37:52-68.
2. Kobayashi H, Komanoya T, Guhaa SK, Haraa K, Fukuoka A. Conversion of cellulose into renewable chemicals by supported metal catalysis. Appl. Catal. A:Gen. (2011) 410:13-20.
3. Pushkarev VV, Musselwhite N, An K, Alayoglu S, Somorjai G. High Structure Sensitivity of Vapor-Phase Furfural Decarbonylation/Hydrogenation Reaction Network as a Function of Size and Shape of Pt Nanoparticles. Nano Lett. (2012) 12:5196-5201.
4. Auer E, Freund A, Pietsch J, Tacke T. Carbons as supports for industrial precious metal catalysts. Appl. Catal. A Gen. (1998) 173:259-271.
5. Xu Z, Xiao FS, Purnell SK, Alexeev O, Kawi S, Deutsch S.E, Gates B.C. Size-dependent catalytic activity of supported metal clusters. Nature (1994) 372:346–348.
6. Boudart M, Djega-Mariadassou G. Kinetics of Heterogeneous Catalytic Reactions. Princeton University Press (1994).

7. Wenderich K, Mul G. Methods, mechanism, and applications of photodeposition in photocatalysis: a review. Chem. Rev. (2016) 116:14587-14619.
8. Pinna F. Supported metal catalysts preparation. Catal. Today (1998) 41:129-137.
9. Crisafulli C, Scirè S, Giuffrida S, Ventimiglia G, Lo Nigro R. An investigation on the use of liquid phase photo-deposition for the preparation of supported Pt catalysts. Appl. Catal. A Gen. (2006) 306:51-57.
10. Tanaka A, Sakaguchi S, Hashimoto K, Kominami H. Preparation of Au/TiO_2 exhibiting strong surface plasmon resonance effective for photoinduced hydrogen formation from organic and inorganic compounds under irradiation of visible light. Catal. Sci. Technol. (2012) 2:907-909.
11. Tanaka A, Sakaguchi S, Hashimoto K, Kominami H. Photocatalytic reactions under irradiation of visible light over gold nanoparticles supported on titanium(IV) oxide powder prepared by using a multi-step photodeposition method. Catal. Sci. Technol. (2014) 4:1931-1938.
12. Camposeco R, Castillo S, Mejia-Centeno I, Navarrete J., Marin J. Characterization of physicochemical properties of Pd/TiO_2 nanostructured catalysts prepared by the photodeposition method. Mater. Charact. (2014) 95:201-210.
13. Dobosz A, Sobczyński A. The influence of silver additives on titania photoactivity in the photooxidation of phenol. Water Res. (2003) 37:1489-1496.
14. Parastar S, Nasseri S, Borji SH, Fazlzadeh M, Mahvi A.H, Javadi A.H, Gholami M. Application of Ag-doped TiO_2 nanoparticle prepared by photodeposition method for nitrate photocatalytic removal from aqueous solutions. Desalin. Water Treat. (2013) 51:7137-7144.
15. Maicu M, Hidalgo MC, Colón G, Navío JA. Comparative study of the photodeposition of Pt, Au and Pd on pre-sulphated TiO_2 for the photocatalytic decomposition of phenol. J. Photochem. Photobiol. A Chem. (2011) 217:275-283.
16. Maeda K, Lu D, Teramura K, Domen K. Simultaneous photodeposition of rhodium–chromium nanoparticles on a semiconductor powder: structural characterization and application to photocatalytic overall water splitting. Energy Environ. Sci. (2010) 3:470-477.
17. Lennox AJJ, Bartels P, Pohl MM, Junge H, Beller M. In situ photodeposition of copper nanoparticles on TiO_2: Novel catalysts with facile light-induced redox cycling. J. Catal. (2016) 340:177-183.
18. Wu G, Guan N, Li L. Low temperature CO oxidation on Cu–Cu_2O/TiO_2 catalyst prepared by photodeposition. Catal. Sci. Technol. (2011) 1:601.
19. Han Y, Zhou J, Wang W, Wan H, Xu Z, Zheng S, Zhu D. Enhanced selective hydrodechlorination of 1,2-dichloroethane to ethylene on Pt–Ag/TiO_2 catalysts prepared by sequential photodeposition. Appl. Catal. B, Environ. (2012) 125:172-179.
20. Ruppert A.M, Weinberg K, Palkovits R. Hydrogenolysis goes bio: from carbohydrates and sugar alcohols to platform chemicals. Angew. Chemie (2012) 51:2564-2601.
21. Li TL., Cai CD, Yeh TF, Teng H. Capped $CuInS_2$ quantum dots for H_2 evolution from water under visible light illumination. J. Alloys Compd. (2013) 550:326-330.
22. Grabowska E, Diak M, Klimczuk T., Lisowski W, Zaleska-Medynska A. Novel decahedral TiO_2 photocatalysts modified with Ru or Rh NPs: insight into the mechanism. J. Mol. Catal. (2017) 434:154-166.
23. Rufus IB, Ramakrishnan V, Viswanathan B, Kuriacose JC. Interface and surface analysis of Ru/CdS. J Mat Sci Lett (1996) 15:1921-1923.
24. Sobczynski A, Jakubowska T, Zielinski S. Hydrogen Photoevolution from Water-Methanol on Ru/TiO2. Monatshefte Fur Chemie Chem. Mon. (1989) 120:101-109.
25. Doniach S, Sunjic M. Many-electron singularity in X-ray photoemission and X-ray line spectra from metals. J. Phys. C Solid State Phys. (1970) 3:285-291.
26. Shirley DA. High-Resolution X-Ray Photoemission Spectrum of the Valence Bands of Gold. Phys. Rev. B. (1972) 5:4709-4714.
27. Wagner CD, Davis LE, Zeller MV, Taylor JA, Raymond RM, Gale LH. Empirical atomic sensitivity factors for quantitative analysis by electron spectroscopy for chemical analysis. Surf. Interface Anal. (1981) 3:211-225.
28. Ruppert AM, Jędrzejczyk M, Sneka-Płatek O, Keller N, Dumon A.S, Michel C, Sautet P, Grams J, Ru catalysts for levulinic acid hydrogenation with formic acid as a hydrogen source. Green Chem. (2016) 18:2014-2028.

29. Coşkuner Filiz B, Gnanakumar ES, Martínez-Arias A, Gengler R, Rudolf P, Rothenberg G, Shiju NR. Highly selective hydrogenation of levulinic acid to γ-Valerolactone over Ru/ZrO_2 catalysts. Catal. Letters (2017) 147:1744-1753.
30. Cabrera NFMN, Mott NF. Theory of the oxidation of metals. Reports on progress in physics (1949) 12:163.
31. Wojciechowska J, Gitzhofer E, Grams J, Ruppert AM, Keller N, Light-driven synthesis of sub-nanometric metallic Ru catalysts on TiO_2. Catalysis Today (2018) https://doi.org/10.1016/j.cattod.2018.07.013
32. Rard J A. Chemistry and Thermodynamics of Ruthenium and Some of Its Inorganic Compounds and Aqueous Species. Chemical Reviews (1985) 85:1-39.
33. Connick RE. Advances in the Chemistry of the Coordination Compounds. Ed. S. Kirschner, Mac Millan (1961).
34. Fine DA. Thesis. University of California at Berkeley (1958).
35. Naya SI, Tanaka M, Kimura K, Tada H. Visible-Light-Driven Copper Acetylacetonate Decomposition by $BiVO_4$. Langmuir (2011) 27:10334-10339.
36. Ruppert AM, Grams J, Jędrzejczyk M, Matras-Michalska J, Keller N, Ostojska K, Sautet P. Titania-Supported Catalysts for Levulinic Acid Hydrogenation: Influence of Support and its Impact on γ-Valerolactone Yield. ChemSusChem. (2015) 8:1538-1547.
37. Cady HH, Connick RE. The Determination of the Formulas of Aqueous Ruthenium (III) Species by Means of Ion-exchange Resin: Ru^{+3}, $RuCl^{+2}$ and $RuC1_2^{+}$. J. Am. Chem. Soc. (1958) 80:2646-2652.
38. Wachala M, Grams J, Kwapinski W, Ruppert AM. Influence of ZrO_2 on catalytic performance of Ru catalyst in hydrolytic hydrogenation of cellulose towards γ-valerolactone. Int J Hydrogen Energy (2016) 41:8688-8695.
39. Ruppert AM, Weinberg, K, Palkovits R. Hydrogenolysis Goes Bio: From Carbohydrates and Sugar Alcohols to Platform Chemicals. Angew. Chem. Int. Ed. (2012) 51(11):2564-2605.
40. Wojciechowska J, Jedrzejczyk M, Grams J, Keller N, Ruppert AM. Enhanced production of γ-valerolactone with internal source of hydrogen on Ca-modified TiO_2 supported Ru catalysts. Chemsuschem (2018) https://doi.org/10.1002/cssc.201801974.